ISSN 1063-7834, Physics of the Solid State, 2008, Vol. 50, No. 11, pp. 2109–2114. © Pleiades Publishing, Ltd., 2008.
Original Russian Text © I.S. Edelman, V.S. Zhigalov, R.D. Ivantsov, V.A. Seredkin, S.M. Zharkov, D.E. Prokof'ev, G.I. Frolov, G.N. Bondarenko, 2008, published in Fizika Tverdogo Tela, 2008, Vol. 50, No. 11, pp. 2021–2026.

MAGNETISM AND FERROELECTRICITY

Structure and the Magnetic and Magneto-Optical Properties of Co–Sm–O Nanogranular Films

I. S. Edelman[a], V. S. Zhigalov[a], R. D. Ivantsov[a], V. A. Seredkin[a, b], S. M. Zharkov[a, b], D. E. Prokof'ev[a], G. I. Frolov[a], and G. N. Bondarenko[c]

[a] *Kirensky Institute of Physics, Siberian Branch, Russian Academy of Sciences, Akademgorodok, Krasnoyarsk, 660036 Russia*
e-mail: ise@iph.krasn.ru

[b] *Siberian Federal University, Svobodnyi pr. 79, Krasnoyarsk, 660041 Russia*

[c] *Institute of Chemistry and Chemical Technology, Siberian Branch, Russian Academy of Sciences, ul. K. Marksa 42, Krasnoyarsk, 660036 Russia*

Received February 28, 2008

Abstract—The magnetic properties and magneto-optical effects in nanocomposites based on Co–Sm–O films prepared through pulsed plasma sputtering of a $SmCo_5$ target are investigated. It is shown that, depending on the technological conditions and regimes of subsequent annealing, the films can have different structures from cobalt nanoparticles distributed in the dielectric samarium oxide matrix with a magnetic phase volume of more than 60% to a continuous polycrystalline cobalt film with embedded samarium oxide nanoparticles. The evolution of the spectra of the magneto-optical Kerr effect and the field dependences of the magnetization is studied as a function of the film structure.

PACS numbers: 75.50.Tt, 75.70.-i, 78.20.Ls

DOI: 10.1134/S1063783408110176

1. INTRODUCTION

Composite materials consisting of magnetic nanoparticles separated by dielectric layers are of considerable interest for both fundamental physics and practical applications. In these materials, a decrease in the particle sizes to a nanometer scale leads to the appearance of new properties, such as the giant magnetoresistance, as well as soft-magnetic and high-resistance properties required by modern engineering [1–3]. These specific features also include a resonance enhancement of magneto-optical effects in different optical ranges, which was predicted theoretically [4, 5] and observed in a number of experimental investigations [6–9].

It is known that the resonance of magneto-optical effects is associated with the localized excitations of free electrons in nanoparticles. Therefore, the parameters of the effects should depend on the particle sizes, the content of the magnetic phase in the composite, and the ratio between the optical parameters of the metal and dielectric. The situation is complicated by the fact that the optical parameters of metal nanoparticles can differ substantially from those of the corresponding bulk materials.

In view of miniaturization problems, special attention, as a rule, has been focused on the study of magneto-optical effects in film composites. It should be noted that films containing the SiO_2 or Al_2O_3 oxides as a dielectric matrix have been predominantly studied to date (see, for example, [6–9]). In our earlier work [10], we for the first time synthesized Co–Sm–O films and investigated their magnetic and structural properties in the initial state and after heat treatments. In these films, samarium occurs as oxide and forms layers between cobalt nanograins. The first results of investigations into the Faraday effect in these samples were published in our previous paper [11]. However, in different applications, developers most frequently have faced geometric parameters of devices at which the use of the Faraday effect is complicated. This raises the problem regarding the study of the Kerr effect in similar materials.

The purpose of this work was to investigate the evolution of the magnetization curves and the spectra of the polar Kerr effect of the samples with a change in their structure due to the change in the technological conditions of the synthesis and subsequent heat treatments.

2. SAMPLE PREPARATION AND EXPERIMENTAL TECHNIQUE

Samples were prepared through pulsed plasma sputtering of a $SmCo_5$ target. The specific feature of this technique is the high pulsed condensation rate (~10^4 nm/s) at a pulse duration of ~10^{-4} s and a high cooling rate of condensates (~10^7 K/s). Since a necessary condition for the preparation of samples with small-sized nanostructured objects is rapid supercooling of the vapors, our technique is an efficient tool for

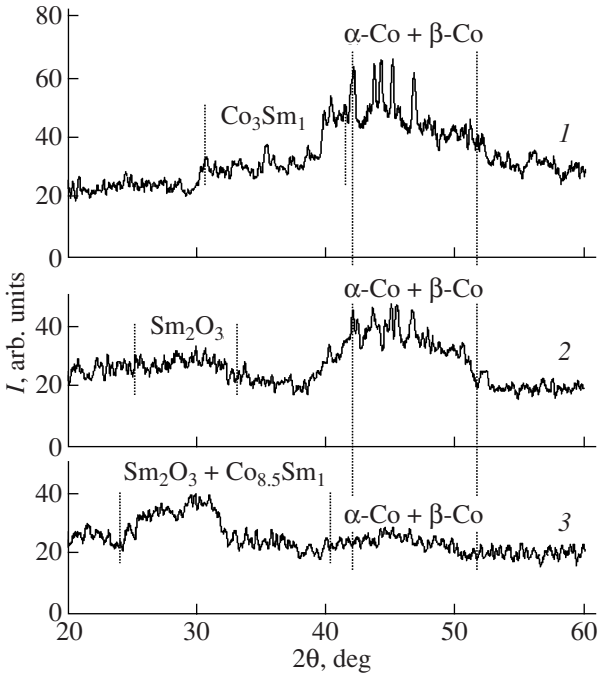

Fig. 1. X-ray diffraction patterns of the initial samples (sample nos. 1–3). Numerals near the curves correspond to the samples numbers.

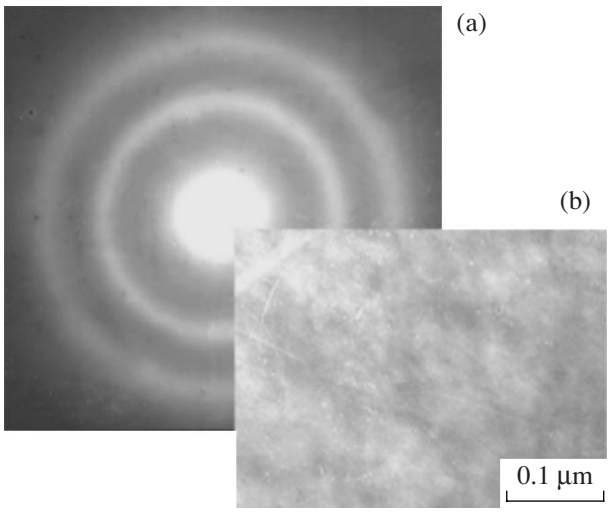

Fig. 2. (a) Electron diffraction pattern and (b) micrograph of a region of sample no. 3.

preparing nanocrystalline films. Moreover, the technique under consideration is characterized by a self-sustaining regime of the existence of a glow-discharge plasma only in vapor of the sputtered metal without additional introduction of a working gas. However, the stability of the plasma and favorable conditions of its existence are improved upon addition of insignificant portions of working gases. In this study, after attainment of an initial residual pressure of 10^{-6} Torr, either argon (sample no. 2) or molecular nitrogen (sample no. 3) was added to a residual pressure of 5×10^{-5} Torr. Sample no. 1 was prepared at a residual pressure of 10^{-9} Torr as a reference sample. The physical and structural properties were measured with the use of as-prepared (initial) samples and the same samples subjected to heat treatments at different temperatures under high vacuum. The duration of each annealing was equal to 30 min.

The newly formed phases and structural transformations were identified using the x-ray diffraction and electron microscopic analyses. The x-ray diffraction patterns were recorded on a DRON-4-07 diffractometer (CuK_α radiation). The electron microscope images of the films were obtained with a PRÉM-200 electron microscope at an accelerating voltage of 100 kV.

The spectral dependences of the polar Kerr effect were measured by the null-analyzer method with the use of the azimuth modulation of the plane of polarization of the light beam in the spectral range 400–950 nm at room temperature. The rotation of the plane of polarization was measured accurate to within ±0.2 min. The magnetic field with a strength of up to 10 kOe was aligned parallel to the light beam perpendicular to the plane of the sample. The accuracy in the measurement of the field strength was ±20 Oe.

The filed dependences of the magnetization were measured on a vibrating-coil magnetometer in magnetic fields with a strength of up to 12 kOe in the directions parallel and perpendicular to the plane of the film. The magnetization was measured accurate to within 3%.

3. EXPERIMENTAL RESULTS AND DISCUSSION

3.1. Structure of the Samples

Owing to the high reactivity of samarium, the structure and properties of the samples depend substantially on the composition of the residual atmosphere in the vacuum chamber. The x-ray diffraction patterns of all three samples are depicted in Fig. 1. The analysis of these x-ray diffraction patterns demonstrates that the composition of sample no. 1 (prepared at a residual pressure of 10^{-9} Torr) contains at least three metal phases, namely, α-Co, β-Co, and the phase approximately identified as Co_3Sm_1, in the complete absence of oxides. The last component is difficultly evaluated because of the small size of structural objects. However, this is not true for the cobalt modifications, because the x-ray diffraction pattern involves pronounced lines of the face-centered cubic and hexagonal close-packed phases of cobalt against a trough-shaped background. The x-ray diffraction pattern of sample no. 2 prepared in the argon atmosphere contains reflections attributed to two cobalt modifications and the compound, most likely, corresponding to the formula $Co_{8.5}Sm_1$. Moreover, a part of samarium manifests

itself in the x-ray diffraction pattern in the form of oxide approximately identified as Sm_2O_3 [12].

The x-ray diffraction pattern of film no. 3 differs substantially from those of film nos. 1 and 2. This pattern contains two halos, i.e., one halo instead of the main reflections of cobalt, and the other halo (more pronounced) corresponds to the samarium oxide [12]. A more accurate identification of the phases in this film is complicated as a result of small sizes of structural particles. In this respect, we performed electron microscopic investigations with a higher resolution. Figure 2 shows the electron diffraction pattern (Fig. 2a) and the micrograph (Fig. 2b) obtained immediately after sputtering of the target. The electron diffraction pattern exhibits two diffuse halos (similar to those observed in the x-ray diffraction pattern) almost with identical intensities. The atomic interplanar distances corresponding to the centers of gravity of the halos are approximately equal to 2.97 and 2.00 Å. A comparison of the data obtained with the x-ray diffraction tables for the cobalt and samarium phases allows us to make the preliminary inference that the reflection corresponding to ~2 Å can be assigned to the face-centered cubic and hexagonal close-packed phases of cobalt or some compounds of cobalt with samarium, for example, $Co_{9.8}Sm_1$ or $Co_{8.5}Sm_1$, as well as cobalt carbides, because the Auger electron spectroscopic data indicate that similar films contain a certain amount of carbon [10]. The diffraction reflection centered at ~2.97 Å is attributed to the hexagonal modification of the Sm_2O_3 phase (JCPDS card no. 19-1114) with the lattice parameters $a = 3.86$ Å and $c = 6.17$ Å [12]. Taking into account the aforesaid, we can assume that the structure of film no. 3 in the initial state represents particles of the cobalt phases (with a maximum size of the order of 2–3 nm) separated by samarium oxide layers (Co–Sm_2O) with a volume of the magnetic phase $f \sim 60\%$ [10, 11].

The performed structural and phase investigations demonstrate that all three samples do not contain the $SmCo_5$ phase corresponding to the composition of the sputtered target and nitrogen compounds. This is explained by the high reactivity of samarium, which completely or partially oxidizes directly in the vacuum chamber during the deposition of the film; in this case, molecular nitrogen remains inert (sample nos. 2, 3).

Annealing of the samples under vacuum leads to significant changes in their structure. Figure 3 depicts the x-ray diffraction patterns of sample no. 3 after annealings at different temperatures. For comparison, x-ray diffraction pattern *1* of this film in the initial state is also shown in Fig. 3. It can be seen from this figure that even the initial stage of annealing (at 510 K, pattern *2*) is accompanied by the transformation of the crystal structure due to the recrystallization (the transition of the magnetic component of the sample from the nanocrystalline state to the polycrystalline sate). The resulting

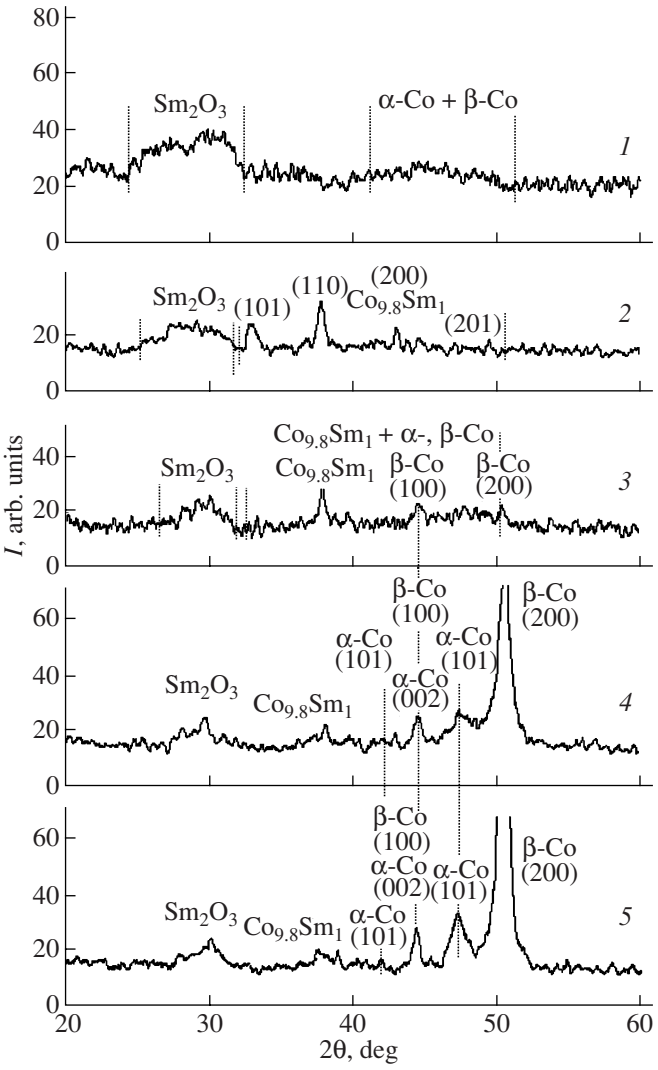

Fig. 3. X-ray diffraction patterns of sample no. 3: (*1*) before annealing and (*2–5*) after annealing at the temperatures T_{ann} = (*2*) 510, (*3*) 610, (*4*) 810, and (*5*) 910 K.

phase can be interpreted as $Co_{9.8}Sm_1$ (JCPDS card no. 47-1896 [12]). Furthermore, the phase of samarium oxide Sm_2O_3 is also involved in the composition of the sample. An increase in the annealing temperature to 610 K (x-ray diffraction pattern *3*) is attended by the appearance of additional reflections, which can be assigned to metallic cobalt (α-Co, β-Co) with almost unchanged contribution of the samarium oxide.

Annealing at higher temperatures (810, 910 K; x-ray diffraction patterns *4*, *5*) results in a radical transformation of the crystal structure with the formation of larger grains of two cobalt modifications (α-Co, β-Co) so that the β-Co phase having a texture oriented in the [200] direction is dominant. The micrograph and the electron diffraction pattern of sample no. 3 annealed at temperatures of 515–780°C are depicted in Fig. 4. The analysis of these data does not permits us to make a unique inference regarding the phase composition of rather

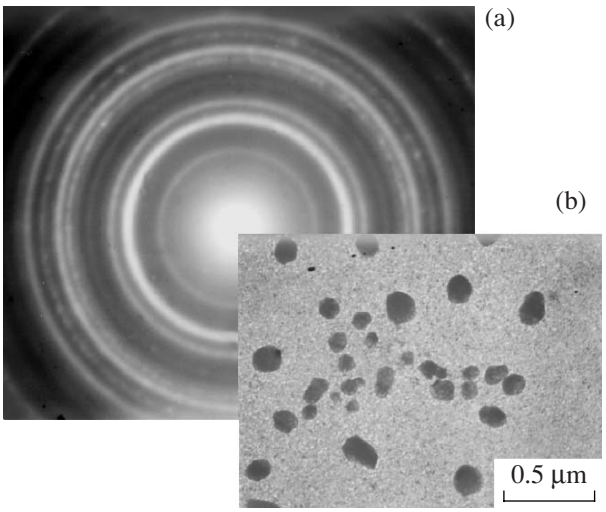

Fig. 4. (a) Electron diffraction pattern and (b) micrograph of a region of sample no. 3 after annealing at a temperature of 780 K.

large particles (70–250 nm in sizes) observed against the background of a more or less homogeneous metal matrix of the sample. A comparison with the x-ray diffraction data enables us to assume that this is the Sm_2O_3 phase (JCPDS card no. 15-0813), even though we cannot completely exclude that these are cobalt particles. Below, we will attempt to elucidate this problem by analyzing the physical properties of the samples under investigation.

Therefore, the used technique provided a means for preparing a series of the samples with different structural features. The samples synthesized in the molecular nitrogen atmosphere turned out to be most sensitive to heat treatments: the state of the samples can be changed from cobalt nanoparticles (possibly, amorphous) embedded in the samarium oxide matrix to a continuous polycrystalline film predominantly consisting of the β-Co phase with inclusions of relatively large particles with an unclear nature (most likely, samarium oxide).

3.2. Magneto-Optical and Magnetic Properties

The dispersion curves of the Kerr effect $Q(\lambda)$ for initial sample nos. 1–3 are depicted in Fig. 5a. It can be seen from this figure that the dependences $Q(\lambda)$ for these samples differ from each other. For the first sample (curve *1*), the dependence $Q(\lambda)$ exhibits a monotonic behavior, the magnitude of the Kerr effect increases with an increase in the wavelength, and the sign of the Kerr effect is negative in the wavelength range under investigation. This dependence is similar to the spectrum of the polar Kerr effect obtained in [13]. However, in [13], the maximum magnitude of the effect is two times larger than that for sample no. 1 and the effect does not change sign. It should be noted that the

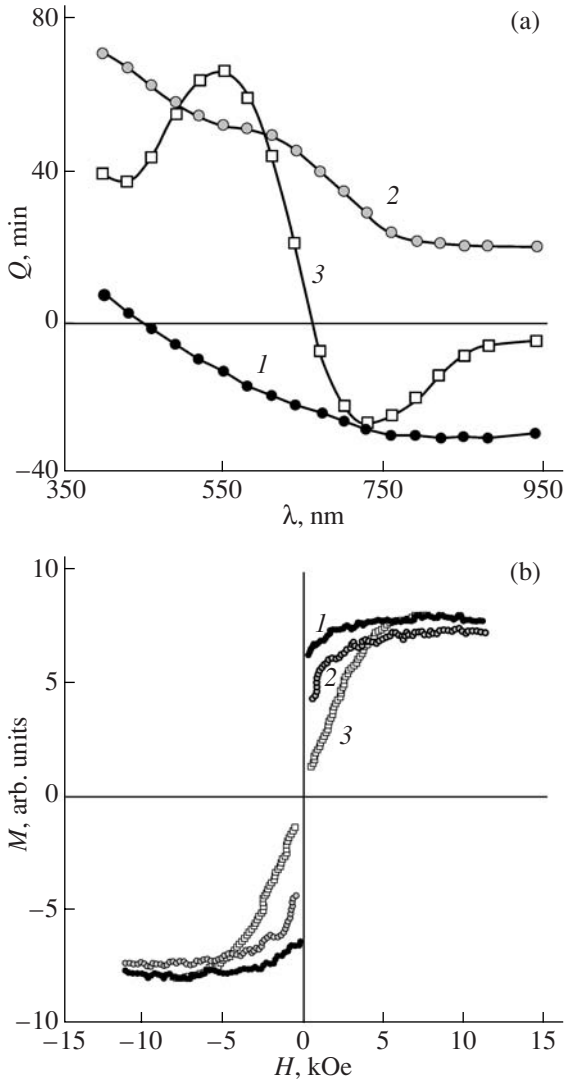

Fig. 5. (a) Dispersion curves for the Kerr effect and (b) field dependences of the magnetization for initial sample nos. (*1*) 1, (*2*) 2, and (*3*) 3.

maximum magnitude of the Kerr effect for sample no. 1 is close to the maximum magnitude of the Kerr effect for epitaxial films of the face-centered cubic and hexagonal close-packed phases of cobalt [14]. However, the change in sign in the short-wavelength range is also not observed in [14]. We can assume that the change in sign can be associated with the contribution from the cobalt alloy with samarium to the Kerr effect. However, this tendency more clearly manifests itself for sample no. 2 to a change in sign over the entire spectral range under investigation (Fig. 5a, curve *2*). For this sample, the reflections of the Co_3Sm_1 phase disappear, but the reflections of the Sm_2O_3 phase become pronounced (Fig. 1, curve *2*). Finally, the spectral dependence of the Kerr effect for sample no. 3 has a resonance character (Fig. 5a, curve *3*) with the change in sign in the vicinity of 650 nm, which, in principle, is consistent with the

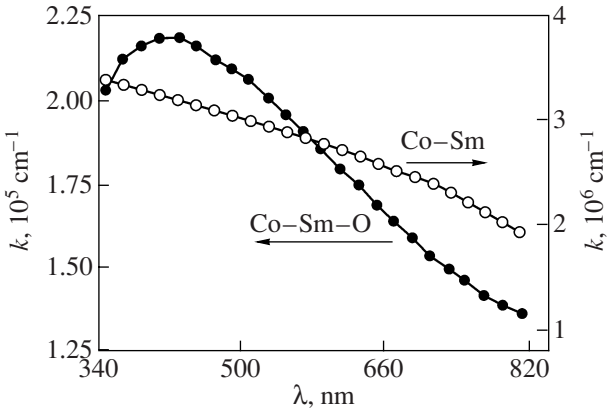

Fig. 6. Optical absorption spectra for initial sample nos. 1 and 3 (Co–Sm and Co–Sm–O, respectively).

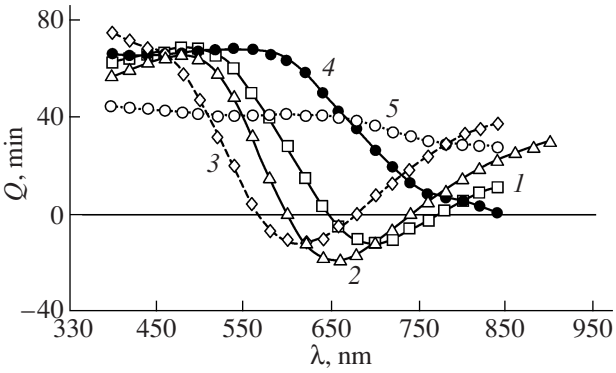

Fig. 7. Spectral dependences of the Kerr effect for sample no. 3: (*1*) before annealing and (*2–5*) after annealing at the temperatures T_{ann} = (*2*) 510, (*3*) 610, (*4*) 810, and (*5*) 910 K.

theoretical predictions for the spectral dependences of the magneto-optical effects in ensembles of metal particles embedded in dielectric matrices [4, 5]. This is in agreement with the inference made in the discussion of the x-ray diffraction data that sample no. 3 consists of cobalt phase nanograins separated by dielectric layers of samarium oxide.

Sample no. 3 is characterized by a drastic increase in the electrical resistivity equal to 5×10^{-2} Ω cm, which is approximately four orders of magnitude higher than the electrical resistivities typical of metal film samples of the same composition prepared under ultrahigh vacuum and almost three orders of magnitude higher than the electrical resistivity of the films synthesized after blow with argon [10, 15]. The presence of dielectric layers and small sizes of cobalt nanoparticles can also lead to a decrease in the optical absorption coefficient, which is actually observed in experiments. Figure 6 shows the optical absorption spectra of two samples. As can be seen from Fig. 6, the absorption coefficient of the sample prepared in the nitrogen atmosphere is nearly one order of magnitude smaller than that of the sample synthesized under ultrahigh vacuum.

These significant differences between the structures of the samples are also responsible for different field dependences of the magnetization. Figure 5b depicts the field dependences of the magnetization for three initial samples in the magnetic field oriented in the plane of the films. For sample nos. 1 and 2, the field dependences of the magnetization for these two geometries differ from each other, which is characteristic of ferromagnetic samples with an in-plane magnetic anisotropy. This circumstance and relatively low saturation fields upon magnetization in the plane allow us to argue that sample nos. 1 and 2 exhibit a ferromagnetic ordering; i.e., even if these samples are nanogranular, the grain number density in the matrix exceeds the percolation threshold. For sample no. 3, the magnetization curve shape similar to the shape of the Langevin curve and a substantially higher saturation field enable us to consider this sample as an ensemble of superparamagnetic nanoparticles of different cobalt phases in the Sm_2O_3 matrix. It should be noted that the nanoparticle number density is below the percolation threshold.

Now, we consider the influence of sequential annealings on the magnetic and magneto-optical properties of the films under investigation. The dispersion curve and the magnitude of the Kerr effect for film no. 1 hardly depend on the annealing temperature. These characteristics weakly depend on the heat treatment for film no. 2 and significantly change for film no. 3. Figure 7 depicts the series of the dependences of the Kerr effect for sample no. 3 in the initial state (curve *1*) and after annealings at different temperatures. Annealing at temperatures of 510 and 610 K (curves *2*, *3*) leads to a shift of the spectral dependences toward the short-wavelength range of the optical spectrum with an insignificant transformation of the curve shape. An increase in the annealing temperature to 810 K and above (curves *4*, *5*) is accompanied by a shift of the dependences in the opposite direction and a change in the curve shape. After annealing at the highest temperature used, the magnitude of the Kerr effect becomes nearly constant over the spectral range under investigation.

Heat treatment of the samples also favors a change in the magnetic and electrical properties. As the annealing temperature increases, sample no. 3 transforms from the superparamagnetic state into the state with the ferromagnetic ordering: the field dependence of the magnetization becomes similar to that for initial sample no. 1 (Fig. 5b), and the saturation magnetization increases by a factor of three. The coercive force exhibits a complex behavior. Initial annealings (at 510, 610 K) lead to the appearance of the hysteresis loop with H_C = 0.1–2.0 Oe. With a further increase in the annealing temperature, the coercive force H_C increases by a factor of several hundreds and reaches a value of 450 Oe.

All these changes can be associated with the recrystallization even at initial annealing temperatures. In the

sample, there appear larger structural fragments, which favor the transformation from the superparamagnetic state to the blocked state with the formation of the hysteresis loop and small coercive forces H_C; however, the dielectric layers around metal grains of cobalt and its compounds with samarium are retained. This assumption can also be made from the analysis of the results of measurements of the electrical resistivity, which remains unchanged as compared to the initial resistivity ρ.

As can be judged from the change in the spectra of the Kerr effect and the large coercive force H_C, the sample at annealing temperatures $T_{ann} > 800$ K passes through the percolation threshold and the long-range magnetic order is established over the entire volume of the sample. These annealings results in a sharp decrease in the electrical resistivity by almost three orders of magnitude as compared to that for the initial sample. In this case, we are dealing with inclusions of dielectric grains in the magnetic matrix rather than with the dielectric layers between magnetic grains. The same inference follows from the x-ray diffraction and electron microscopic data (Figs. 3, 4).

4. CONCLUSIONS

Thus, it was demonstrated that the Co–Sm–O films synthesized by pulsed plasma sputtering of a $SmCo_5$ target in a molecular nitrogen atmosphere have a granulated composite structure, which consists of ferromagnetic metal particles in a dielectric matrix with a large volume of the magnetic phase (~60%).

The magnetic properties of the film samples under investigation exhibit a specific spectral dependence and differ substantially from those of the films prepared by sputtering the same alloy under ultrahigh vacuum and vacuum after blow with argon. The possibility of synthesizing nanogranular samples with specific magnetooptical, magnetic, and electrical properties (such as the soft-magnetic properties, high magnetization, high resistance, small absorption coefficient, and large Kerr rotation in the short-wavelength spectral range) has aroused additional interest in these films from the applied viewpoint. A combination of magnetic properties and a high electrical resistivity makes film objects interesting for practical applications, for example, in high-frequency engineering.

ACKNOWLEDGMENTS

We would like to thank G.V. Bondarenko for the performance of the x-ray fluorescence measurements of the samples under investigation.

This study was supported by the Russian Foundation for Basic Research (project no. 07-02-92174) and performed within the framework of the Program "Development of the Scientific Potential of the Higher School" (project no. 2.1.1.7376). R.D. Ivantsov acknowledges the support of the Russian Science Support Foundation.

REFERENCES

1. F. Parent, Phys. Rev. B: Condens. Matter **55**, 3683 (1997).
2. D. E. Lood, J. Appl. Phys. **38**, 5089 (1967).
3. P. H. Lissberger and P. W. Saunders, Thin Solid Films **34**, 333 (1976).
4. T. K. Xia, P. M. Hui, and D. Stroud, J. Appl. Phys. **67**, 2736 (1990).
5. E. A. Gan'shina, M. V. Vashuk, A. N. Vinogradov, A. B. Granovsky, V. S. Gushchin, P. N. Shcherbak, Yu. E. Kalinin, A. V. Sitnikov, Chong-Oh Kim, and Cheol Gi Kim, Zh. Éksp. Teor. Fiz. **125** (5), 1172 (2004) [JETP **98** (5), 1027 (2004)].
6. Yu. A. Dynnik, I. S. Édel'man, T. P. Morozova, P. D. Kim, I. A. Turpanov, and A. Ya. Beten'kova, Zh. Nauchn. Prikl. Fotogr. **43** (5), 18 (1998).
7. E. Gan'shina, A. Granovsky, B. Dieny, M. Kumaritova, and A. Yurasov, Physica B (Amsterdam) **229**, 260 (2001).
8. I. B. Bykov, E. A. Gan'shina, A. B. Granovskiĭ, and V. S. Gushchin, Fiz. Tverd. Tela (St. Petersburg) **42** (3), 487 (2000) [Phys. Solid State **42** (3), 498 (2000)].
9. A. B. Granovsky, I. V. Bykov, E. A. Gan'shina, V. S. Gushchin, M. Inoue, Yu. E. Kalinin, A. A. Kozlov, and A. N. Yurasov, Zh. Éksp. Teor. Fiz. **123** (6), 1256 (2003) [JETP **96** (6), 1104 (2003)].
10. G. I. Frolov, V. S. Zhigalov, S. M. Zharkov, A. I. Pol'skiĭ, and V. V. Kirgizov, Fiz. Tverd. Tela (St. Petersburg) **45** (12), 2203 (2003) [Phys. Solid State **45** (12), 2303 (2003)].
11. V. S. Zhigalov, R. D. Ivantsov, I. S. Édel'man, V. A. Seredkin, G. I. Frolov, and G. V. Bonadrenko, Fiz. Tverd. Tela (St. Petersburg) **47** (6), 1092 (2005) [Phys. Solid State **47** (6), 1129 (2005)].
12. *Powder Diffraction File* (Joint Committee on Powder Diffraction Standards—International Center for Diffraction Data, Swarthmore, PA, United States).
13. K. H. J. Buschow, P. G. van Engen, and R. Jongebreur, J. Magn. Magn. Mater. **38**, 1 (1983).
14. D. Weller, G. R. Harp, R. F. C. Farrow, A. Cebollada, and J. Sticht, Phys. Rev. Lett. **72**, 2097 (1994).
15. V. S. Zhigalov, G. I. Frolov, and L. I. Kveglis, Fiz. Tverd. Tela (St. Petersburg) **40** (11), 2074 (1998) [Phys. Solid State **40** (11), 1878 (1998)].

Translated by O. Borovik-Romanova